Front. Earth Sci. 2022, 16(1): 75–89
https://doi.org/10.1007/s11707-020-0838-9

RESEARCH ARTICLE

Validation of Doppler Wind Lidar during Super Typhoon Lekima (2019)

Shengming TANG[1,2], Yun GUO[3], Xu WANG (✉)[3], Jie TANG[1], Tiantian LI[1], Bingke ZHAO[1], Shuai ZHANG[1], Yongping LI[1]

1 Shanghai Typhoon Institute of China Meteorological Administration, Shanghai 200030, China
2 Key Laboratory of Numerical Modeling for Tropical Cyclones, China Meteorological Administration, Shanghai 200030, China
3 State Key Laboratory of Mountain Bridge and Tunnel Engineering, Chongqing Jiaotong University, Chongqing 400074, China

Abstract This study undertook verification of the applicability and accuracy of wind data measured using a WindCube V2 Doppler Wind Lidar (DWL). The data were collected as part of a field experiment in Zhoushan, Zhejiang Province (China), which was conducted by Shanghai Typhoon Institute of China Meteorological Administration during the passage of Super Typhoon Lekima (2019). The DWL measurements were compared with balloon-borne GPS radiosonde (GPS sonde) data, which were acquired using balloons launched from the DWL location. Results showed that wind speed measured by GPS sonde at heights of < 100 m is unreliable owing to the drift effect. Optimal agreement (at heights of > 100 m) was found for DWL-measured wind speed time-averaged during the ascent of the GPS sonde from the ground surface to the height of 270 m (correlation coefficient: 0.82; root mean square (RMS): 2.19 $m \cdot s^{-1}$). Analysis revealed that precipitation intensity (PI) exerts considerable influence on both the carrier-to-noise ratio and the rate of missing DWL data; however, PI has minimal effect on the wind speed bias of DWL measurements. Specifically, the rate of missing DWL data increased with increasing measurement height and PI. For PI classed as heavy rain or less ($PI < 12$ $mm \cdot h^{-1}$), the DWL data below 300 m were considered valid, whereas for PI classed as a severe rainstorm ($PI > 90$ $mm \cdot h^{-1}$), only data below 100 m were valid. Up to the height of 300 m, the RMS of the DWL measurements was nearly half that of wind profile radar (WPR) estimates (4.32 $m \cdot s^{-1}$), indicating that DWL wind data are more accurate than WPR data under typhoon conditions.

Keywords Lidar, WindCube, GPS sonde, Super Typhoon Lekima, precipitation

Received June 13, 2020; accepted September 28, 2020

E-mail: tangsm@typhoon.org.cn, xuwang@cqjtu.org.cn

1 Introduction

Tropical cyclones are among the most destructive of natural disasters. Eight of the 10 disaster events that caused the greatest economic losses have been related to tropical cyclones (Yu and Chen, 2019). Typhoon-related wind, especially the wind in the boundary layer, is an important variable in various fields such as aerospace, wind energy assessment, civil engineering, and transportation (Hannon, 2000; Powell et al., 2003; Courtney et al., 2008; Zheng et al., 2015). However, historically, the typhoon boundary layer has been the least comprehensively observed part of such storms (Zhang et al., 2018).

The most effective way to characterize typhoon wind in the boundary layer is through *in situ* observation. Generally, such observations can be obtained using two approaches: passive and active measurement. Passive measurement includes using buoys, vanes, and anemometers that can capture high-frequency winds at a single point. Wind towers with several vanes and anemometers installed at different heights can provide wind profile information. However, the high construction and maintenance costs, lack of mobility, and restricted height of measurements of such towers (usually < 150 m) limit their widespread application to studies of tropical cyclones. A balloon-borne GPS radiosonde (GPS sonde) or GPS dropsonde collects instantaneous wind speed data along its track, which can extend as far as a few tens of kilometers. However, a GPS sonde cannot obtain a time series of a wind profile. The wind profile radar (WPR) and Doppler wind lidar (DWL) are both sensors that can provide active measurements of wind. However, related studies have shown that the data quality of WPR measurements is easily affected by heavy rainfall (Ralph et al., 1995; Lambert and Taylor, 1998).

Use of a DWL can overcome the limitations of sampling height and poor mobility associated with a wind tower. A

DWL can sample multiple points synchronously with high spatial and temporal resolutions and anti-interference capability, which is highly advantageous in comparison with other measurement techniques. Relevant studies have shown that DWL has high reliability in measuring regular climatological wind. For example, Peña et al. (2009) observed offshore wind for a six-month period. Comparison of their DWL-derived mean wind speed with cup anemometer data obtained at the height of 63 m showed high correlation for the open sea region, i.e., the correlation coefficient (CORR) was >0.97 and the slope of the linear regression was approximately 1.0. Köpp et al. (1984) compared field wind data obtained at heights of 100, 350, and 750 m measured by both a continuous wave DWL and a GPS sonde. Analysis of these two data sets revealed that the CORR could reach 0.83 (0.91) and that the root mean square (RMS) was 1.3 $m \cdot s^{-1}$ (12°) for wind speed (direction). Roadcap et al. (2001) compared the wind speeds measured by a CO_2 DWL and GPS sonde as a function of altitude up to 6 km, and reported that the CORR was >0.81 and that the RMS was within 1.95 $m \cdot s^{-1}$. Wolfe et al. (2005) analyzed the observational capability of DWL and WPR at sea level, as well as that of GPS sondes. Their results confirmed that DWL could compensate for the limitation of a WPR in terms of the minimum measurement range. The CORR between the DWL and GPS sonde wind speeds was >0.97, and the accuracy of the DWL-derived wind speed was approximately 0.1 $m \cdot s^{-1}$. Kumer et al. (2014) compared wind data measured by two types of DWL (i.e., WindCube V1 and WindCube 100S) with GPS sonde data acquired at the same site. The wind speed data of the WindCube 100S and GPS sonde showed a high degree of correlation (CORR $>$ 0.93) between 0.15 and 2.5 km; the CORR between the WindCube V1 and GPS sonde was >0.7 within the height range of 70–250 m. Thus, for regular climatological wind observed by a DWL, the above studies showed that the CORR of wind speed (direction) was generally >0.7 (>0.9) and the RMS was within 1–2 $m \cdot s^{-1}$ (10°).

The first use of DWL as part of a tropical cyclone mission was in the THORPEX Pacific Asian Regional Campaign in 2008. Pu et al. (2010) presented the results of airborne DWL measurements obtained during Typhoon Nuri (2008). The accuracy of the typhoon observational data measured by the airborne DWL was verified by comparison with GPS dropsonde data. The airborne DWL observations agreed well with the GPS dropsonde data with values of CORR and bias of 0.977 and 0.36 $m \cdot s^{-1}$, respectively. Emmitt (2010) conducted extensive studies of tropical cyclones using an airborne DWL. Although the coherent DWL depended upon atmospheric aerosol particles for its return signal, the vertical coverage varied from one situation to another. Generally, the wind profile within 3 km above the ground could be obtained, and accurate wind profiles under typhoon and cloudy conditions were observed by the DWL. Based on data obtained by a coherent DWL aboard a P3 Hurricane Hunter aircraft of the National Oceanic and Atmospheric Administration, Zhang et al. (2018) analyzed wind profile data collected during Tropical Storm Erika (2015). Comparison of airborne DWL observations and winds measured by GPS dropsondes showed that the CORR between these two data sets was 0.95 and that the RMS was 1.58 $m \cdot s^{-1}$. Bucci et al. (2018) compared wind observations from an airborne DWL with GPS dropsonde data obtained during tropical cyclones in 2016. Although the GPS dropsonde and airborne DWL locations were separated by an average distance of 4.55 km, the CORR of the measured wind speed (direction) was 0.959 (0.917). Moreover, the average wind speed bias was 10.27 $m \cdot s^{-1}$ and the RMS of the wind direction was 40.66°.

Precipitation can affect both the range and the accuracy of DWL detection. However, when precipitation intensity (PI) is <1.5 $mm \cdot h^{-1}$, an increase of PI will improve the efficiency of DWL detection (Matvienko et al., 1995). In an evaluation of the performance of DWL, raindrops were found likely to contribute to the Doppler signal (Smith et al., 2006). Nevertheless, it was considered that the horizontal component of wind velocity in the study could have been susceptible to overestimation because the raindrops fell through a shear gradient and took some time to reach their ultimate velocity. However, there was no specific analysis concerning the impact of precipitation on wind speed measurements derived by DWL. Träumner et al. (2009) investigated wind data measured by both a 2-μm DWL and a 35.5-GHz cloud radar. Their analysis found no significant differences between the wind speeds observed by the two systems in clear sky conditions. During rain events, double peaks were detected in the Doppler spectra of the lidar, and the mean velocity derived from the radar data was lower than that obtained from the DWL. Rabadan et al. (2010) investigated the detection performance of an airborne DWL. Their results proved that wind speed could be observed under flight-test conditions up to heights of around 11.9 km under conditions of clear air, rain, dense clouds, and ice rain with a standard deviation of approximately 1.0–1.5 $m \cdot s^{-1}$. Davis et al. (2013) analyzed the wind profile measured by an airborne DWL when convective precipitation occurred, and it was considered that the precipitation caused aerosol particles to move downward. However, the actual wind speed was low during the observational period, and there was no further discussion regarding the error of the DWL measurements obtained under conditions of precipitation. Kumer et al. (2014) highlighted that DWL measurements of wind speed are highly sensitive to change of weather conditions; however, no analysis of the detection capability of DWL under conditions of precipitation was reported.

Based on field experiments conducted during Super Typhoon Lekima (2019), this study investigated the applicability and accuracy of DWL under conditions of high winds and heavy precipitation. The DWL-derived

wind measurements were compared with GPS sonde and WPR data to provide a reference regarding the application of DWL under typhoon conditions.

The remainder of this paper is organized as follows. Section 2 briefly introduces the pertinent facts of Super Typhoon Lekima and the field experiments. Section 3 describes the instrument settings used for the field experiment, including the DWL, GPS sonde, and WPR, as well as the associated measurement principles and the carrier-to-noise ratio (CNR). Section 4 evaluates the applicability and accuracy of the DWL-derived wind measurements in comparison with the GPS sonde and WPR data obtained under conditions of combined high winds and heavy precipitation. Finally, Section 5 presents a discussion and our conclusions.

2 Field experiment during Super Typhoon Lekima

2.1 Super Typhoon Lekima (2019)

Super Typhoon Lekima, the ninth named storm of the 2019 Pacific typhoon season, developed from a tropical depression that formed east of the Philippines and strengthened to its peak intensity as a super typhoon (>50.9 m s^{-1}) late on August 7, 2019. At around 01:45 CST (China Standard Time: CST = UTC + 08) on August 10, Lekima made landfall over Wenling, Zhejiang Province (China), with maximum wind speeds of up to 52 m·s^{-1} (Force 16 on the Beaufort Wind Scale) and a minimum sea level pressure of 930 hPa. Thereafter, Lekima swept through Zhejiang and Jiangsu provinces and moved away across the Yellow Sea. At around 20:50 CST on August 11, Lekima made its second landfall in Qingdao, Shandong Province, and then meandered away across the Shandong Peninsula and the Bohai Sea. The best-track positions and intensities of Lekima from 02:00 CST on August 4 to 20:00 CST on August 14 are shown in Fig. 1; the data set was obtained from the China Meteorological Administration's best-track database (Ying et al., 2014). The location of the field experiment conducted during the passage of Typhoon Lekima is indicated by the black star in Fig. 1.

Lekima was characterized by its high intensity, severe precipitation, and extended duration over land. First, Lekima was the fifth strongest typhoon on record to make landfall over China. The maximum observed surface wind of 61.4 m·s^{-1} was recorded on the island of Sansuan; this was the second-highest wind speed ever recorded in

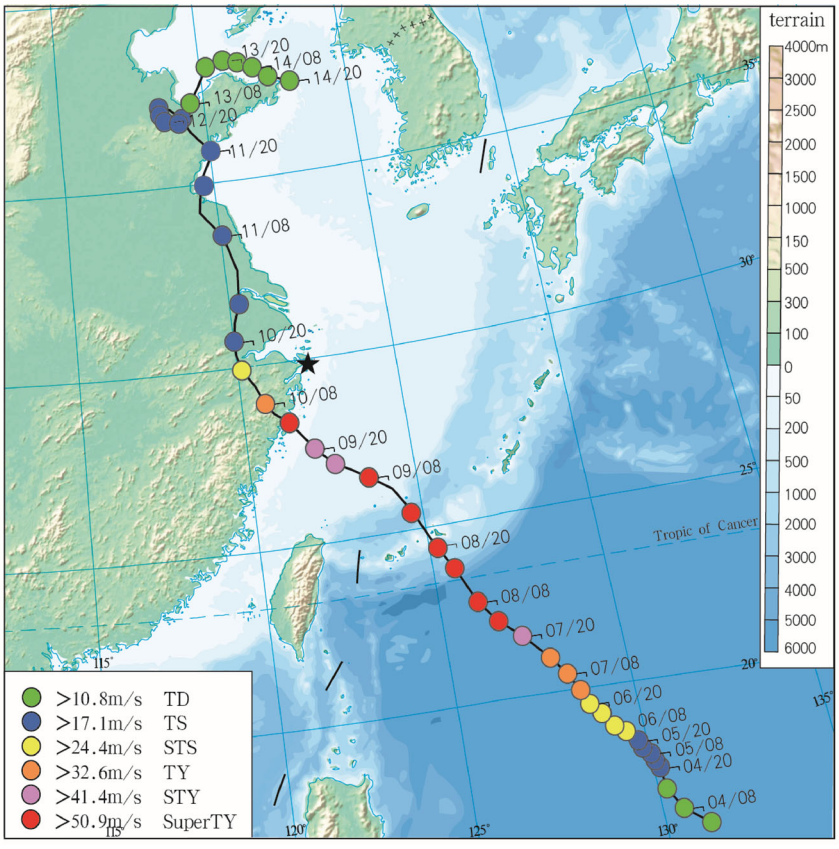

Fig. 1 Best-track positions of Super Typhoon Lekima on August 4–13, 2019. Different colors represent different intensities (GB/T 19201–2006). Super TY: super typhoon; STY: severe typhoon; TY: typhoon; STS: severe tropical storm; TS: tropical storm; and TD: tropical depression. Black star represents the location of the field experiment.

Zhejiang Province. Second, Lekima brought a substantial amount of precipitation. Altogether, 19 weather stations in both Zhejiang (on August 9) and Shandong (on August 11) provinces broke their daily precipitation records. During the passage of Typhoon Lekima, the accumulated precipitation averaged across Shandong and Zhejiang provinces was approximately 158 and 165 mm, respectively, ranking first and second in the history of the two provinces. Specifically, the accumulated precipitation at Kuocang Mountain, Linhai, was 831 mm. Third, owing to its low speed of movement and extended duration over land, Lekima brought widespread destruction along its path. Specifically, it persisted over Zhejiang Province for a 20-h period, making it the longest-lasting super typhoon ever observed in the region.

2.2 Field experiment

The field experiment was conducted at the International Cruise Ship Terminal (29.9022°N, 122.3674°E) in Zhoushan, Zhejiang Province (China), which is denoted by the black star shown in Fig. 1. During the passage of Typhoon Lekima, the shortest distance between the experiment site and typhoon center was 164 km. The experiment site is bordered locally by farmland and sparse buildings on its northern and eastern sides and by the Zhitou Ocean to the south (Fig. 2).

Photographs of the observational instrumentation (i.e., DWL, GPS sonde, and WPR) used in the experiment are also shown in Fig. 2. In addition, precipitation and air temperature data were collected using a 10-m-high vehicle-mounted weather station. Precipitation was recorded at 10-s intervals using raindrop size spectrometers, and air temperature was recorded every 60 s using temperature sensors. It is important to note that all the above observational instruments were deployed at the same location shown in Fig. 2. The observed time series covered a 24-h period from 13:00 CST on August 9 to 13:00 CST on August 10, 2019.

Fig. 2 Photographs showing the local surroundings of the field experiment site and relevant observational instrumentation comprising the DWL, GPS sonde, and WPR.

3 Instrument settings and measurement principles

3.1 Instrument settings

3.1.1 DWL

The DWL used in the study was a WindCube V2 pulsed-type lidar manufactured by Leosphere®, which could continuously measure the three-dimensional wind field and associated standard deviation, CNR, and data availability up to 300 m. It could also measure near-surface air temperature, relative humidity, and air pressure. Measurements were recorded at 12 different heights, i.e., 40, 50, 70, 100, 130, 150, 180, 200, 230, 250, 270, and 290 m. However, the data at 290 m were not included in the analysis because they were deemed invalid. Specifications of the DWL are detailed in Table 1.

Table 1 Specifications of the DWL, GPS sonde, and WPR

Parameter	DWL (WindCube V2)	GPS sonde (Vaisala RS41-SG)	WPR (Airda 3000M)
Measurement range	40–290 m	0–40000 m	50–3000 m
Number of measurement levels	12	–	39
Data sampling rate	1 Hz	0.5 Hz	5 min averaged
Speed accuracy	0.1 $m \cdot s^{-1}$	0.1 $m \cdot s^{-1}$	0.1 $m \cdot s^{-1}$
Speed measurement uncertainty	–	±0.15 $m \cdot s^{-1}$	±1 $m \cdot s^{-1}$ (< 30 $m \cdot s^{-1}$), ±2 $m \cdot s^{-1}$ (30–60 $m \cdot s^{-1}$)
Speed range	0–80 $m \cdot s^{-1}$	0–160 $m \cdot s^{-1}$	0–60 $m \cdot s^{-1}$
Direction accuracy	1°	0.1°	1°
Direction measurement uncertainty	–	±2°	±15°
Temperature range	–35°C – + 45°C	–90°C – + 60°C	–30°C – + 50°C
Humidity range	0%–100% RH	0%–100% RH	0%–90% RH

3.1.2 GPS sonde

During the 24-h observation period, nine sounding balloons were launched at 14:59, 17:12, 19:18, 21:23, and 23:58 CST on August 9 and 02:22, 05:34, 07:07, and 11:50 CST on August 10. The type of radiosonde carried by the sounding balloon was a Vaisala® Radiosonde RS41-SG, which could continuously collect horizontal wind speed and direction, air pressure, air temperature, relative humidity, height, latitude, and longitude. Specifications of the radiosonde are summarized in Table 1.

3.1.3 WPR

In addition to the DWL and GPS sonde, a WPR was also deployed as part of the experiment for comprehensive investigation and validation of the applicability and accuracy of the DWL-derived measurements. The WPR used in the field experiment was an Airda® 3000M vehicle-borne boundary-layer WPR, which could measure continuously both the three-dimensional wind field and the data reliability in the range of 50–3000 m above the ground. The Airda 3000M WPR uses phase demodulation and pulse coding technology with a working frequency of 1290 MHz. It operates with a single vertical beam and four inclined beams with a zenith angle of 15° in two perpendicular directions. Altogether, 39 levels of data were recorded up to the height of 3000 m with vertical resolution of either 50 or 100 m. Specifications of the WPR are also listed in Table 1.

3.2 Measurement principle of DWL

The measurement principle of a DWL relies on the Doppler-induced laser wavelength shift between infrared laser pulses transmitted into the air and the received light backscattered by atmospheric particles (e.g., water droplets, aerosol particles, and dust) (Werner, 1985). The wind profile measurements of the WindCube V2 extend across the range of heights of 40–290 m. Five laser beams are emitted from the DWL: four with inclined lines of sight along a 28° scanning cone angle and a single vertical line of sight (Fig. 3). For each laser beam, the received backscattered light is processed to determine the Doppler shift of the scattered signal, which can be used to calculate the wind velocity along the line of sight using Eq. (1):

$$v_{\mathrm{r}} = \lambda \Delta f / 2, \tag{1}$$

where v_{r} is the radial velocity along the line of sight, λ is the laser wavelength (specified as 1543 nm for the WindCube Lidar), and Δf is the Doppler shift.

The method for retrieval of the horizontal wind using the WindCube lidar is largely the same as the Doppler radar velocity azimuth display algorithm that was first proposed by Lhermitte and Atlas (1961). Assuming that the variation

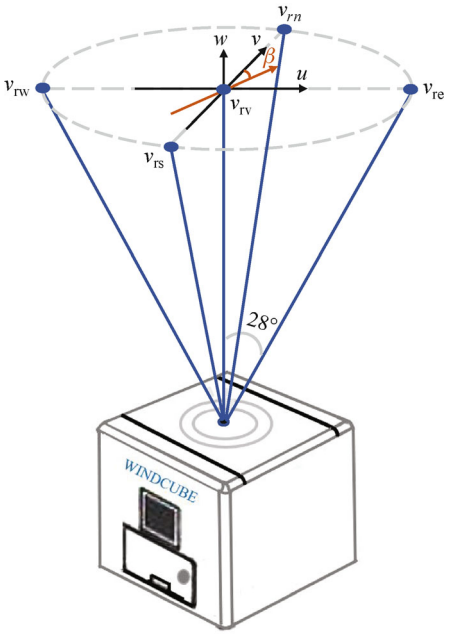

Fig. 3 Schematic of the measurement principle of the WindCube V2 DWL. v_{re}, v_{rs}, v_{rw}, and v_{rn} are radial speeds in the east, south, west, and north directions, respectively, along a 28° scanning cone angle, and v_{rv} is the speed in the vertical direction. u, v, and w are the three wind components in Cartesian coordinates, and β is the horizontal wind direction.

of the horizontal wind is linear above the DWL, the three wind components in Cartesian coordinates can be calculated by applying trigonometric functions as follows:

$$u = \frac{v_{\mathrm{re}} - v_{\mathrm{rw}}}{\sin\theta}, \tag{2}$$

$$v = \frac{v_{\mathrm{rn}} - v_{\mathrm{rs}}}{\sin\theta}, \tag{3}$$

$$w = v_{\mathrm{rv}}, \tag{4}$$

where u, v, and w are the three velocity components in Cartesian coordinates (x, y, z), θ is the angle of the inclined measuring beam off vertical, which was set to $\theta = 28°$ in the experiment. Then, the horizontal total wind speed and direction can be calculated as follows:

$$U = \sqrt{u^2 + v^2}, \tag{5}$$

$$\beta = \arctan(u/v), \tag{6}$$

where U is the horizontal total wind speed, and β is the horizontal wind direction measured clockwise from due north (0°).

3.3 Carrier-to-noise ratio (*CNR*)

The backscattered signal of the coherent WindCube V2

DWL is mixed with system background noises that include short noise (Frehlich and Kavaya, 1991), relative intensity noise (Agrawal, 2010), and thermal noise (Bu et al., 2014):

$$\langle i_n^2 \rangle = \langle i_{\mathrm{SN}}^2 \rangle + \langle i_{\mathrm{T}}^2 \rangle + \langle i_{\mathrm{RIN}}^2 \rangle, \tag{7}$$

where $\langle i_n^2 \rangle$ is the total noise power, $\langle i_{\mathrm{SN}}^2 \rangle$ is the average short noise power, $\langle i_{\mathrm{T}}^2 \rangle$ is the average thermal noise power, and $\langle i_{\mathrm{RIN}}^2 \rangle$ is the average relative intensity noise power.

The *CNR* of the DWL reflects the amount of detected backscattered signal relative to the system background noises, and it is defined as the ratio of the backscattered signal to the total noise:

$$CNR = \frac{\langle i_{het}^2 \rangle}{\langle i_n^2 \rangle}, \tag{8}$$

where $\langle i_{het}^2 \rangle$ is the average direct detection power.

4 Experimental results

Figure 4 presents the time series of 10-min average wind speed and direction of the DWL measurements, rate of missing data, and PI. As shown in Fig. 4(a), the 10-min average wind speed generally increases with height. At most heights, the maximum wind speed was reached at around 09:50 CST on August 9 (i.e., approximately 4 h before landfall). Specifically, the maximum wind speed was 21.7 $\mathrm{m \cdot s^{-1}}$ at 40 m and 30.6 $\mathrm{m \cdot s^{-1}}$ at 270 m. The prevailing wind before 09:50 CST on August 9 was easterly, but it gradually changed to southerly because of the northward movement of the typhoon center after landfall. It should be noted that the wind direction within the range of heights of 40–270 m is largely uniform in the vertical direction. It can be seen from Fig. 4(b) that the rate of missing data increases with both height and PI. Generally, the rates of missing data at heights of < 100 m and within 100–200 m are lower than 20% and 50%, respectively. However, the rate of missing data are higher at heights of > 200 m in periods of heavy rainfall (PI > 25 $\mathrm{mm \cdot h^{-1}}$). At specific times, e.g., around 11:30 and 12:30 CST on August 10, the rate of missing data reached a peak value of up to 100%. The reason for the missing data was weakening of the backscattered signal caused by the increasing detection height and heavier precipitation. With the increase of height, the aerosol concentration lowers and the angular scattering probability of the DWL reduces, which decreases the number of photons received by the DWL. Moreover, heavy rainfall tends to reduce atmospheric transmission of laser light, which further weakens the backscattered signal.

Research on the applicability and accuracy of DWL measurements under the combined effects of high winds and heavy precipitation during super typhoons is lacking. Therefore, a necessary first step was assessment and validation of the DWL measurements obtained during the experiment. A GPS sonde is considered one of the most reliable and accurate systems for wind measurement under the conditions of both high winds and heavy precipitation, and associated measurements have been used extensively as reference data in numerous previous studies (Barat and Cot, 1995; Pu et al., 2010; Zhang et al., 2018). Therefore, in the current study, GPS sondes were deployed to obtain benchmark data with which to assess and validate the DWL-derived measurements.

It should be noted that the wind measurements by the GPS sondes and the DWL were not strictly conducted at the same location. A GPS sounding balloon drifts downwind during its ascent and thus it gradually moves away from the original launch location. Therefore, a GPS sonde

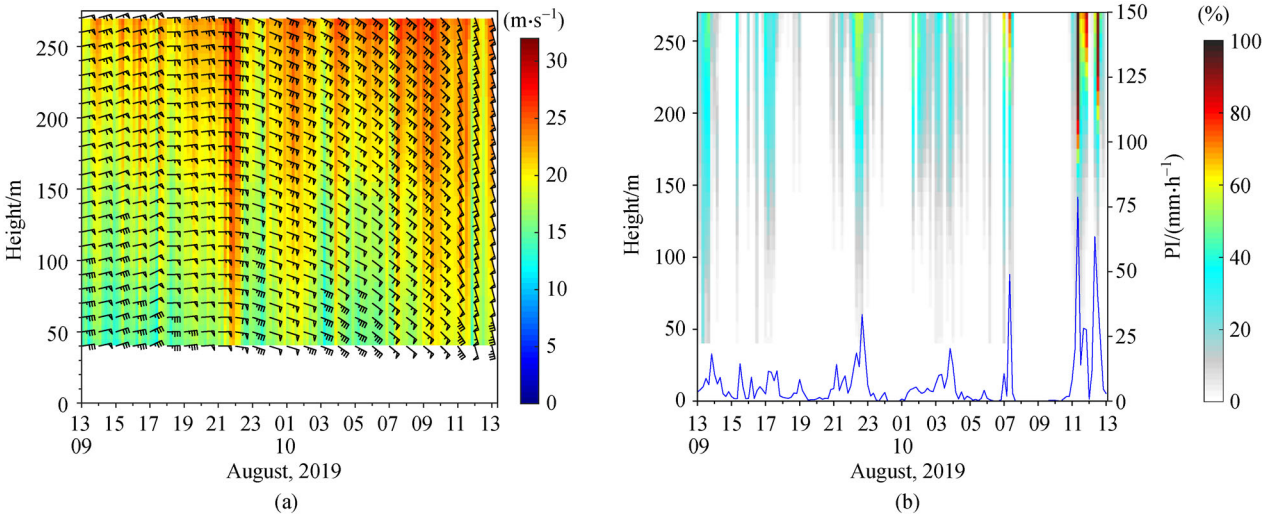

Fig. 4 Time series of (a) 10-min average horizontal wind speed and direction of the DWL measurements, (b) rate of missing data, and PI. The observation period extended from 13:00 CST on August 9 to 13:00 CST on August 10, 2019.

collects instantaneous wind velocity along its drifting track at a fixed time interval (every 2 s). In obtaining DWL measurements, a larger angle off vertical of the inclined beam produces measurements that are more accurate; however, the measuring range in the horizontal direction is also increased. Specifically, the horizontal distance between two opposite inclined beams at the height of 300 m is up to approximately 320 m with an inclined angle of 28°. Consequently, the assumption that variation of the horizontal wind is linear above the DWL is hard to be satisfied in conditions of severely turbulent winds under typhoon conditions. Gasch et al. (2020) suggested that flow inhomogeneity induced by boundary layer turbulence makes an important contribution to the error in DWL measurements and is nonnegligible at low wind velocity. To overcome this problem, time averaging over a certain period is usually applied to eliminate the effects of atmospheric turbulence on measurements of instantaneous wind velocity. Such a strategy was employed in various previous studies. For example, both Li and Yu (2017) and Li et al. (2018) applied 10-min average wind velocities to assess the wind resource over Lake Erie (USA), and Drew et al. (2013) investigated the wind velocity profile during an 8-month observation period based on 1 h average data. The duration of ascent of the GPS sonde from the ground surface to the height of 270 m can be expressed as t_{GPS}. In the current study, 1-s instantaneous, t_{GPS}, 1-min, 2-min, and 10-min average wind speeds and directions derived from the DWL measurements were used to match the GPS sonde data (2-s instantaneous results).

4.1 Assessment of horizontal wind speed

The wind speed profiles of the DWL measurements and GPS sonde data at various time instants, together with the horizontal drift distance of the balloon from its original launch location, are compared in Fig. 5. At heights of < 100 m, the DWL-measured wind speeds are evidently different from those measured by the GPS sondes, although the differences decrease with height. Above approximately 100 m, the DWL measurements are generally in good agreement with the GPS sonde data. This is presumably because, immediately after a balloon is launched, it needs to transform from a static state to traveling at a rate equal to the ambient wind speed. Throughout this initial period, as the balloon accelerates to match the wind speed, the wind speed measured by the balloon is less than the actual speed of the prevailing wind, generating larger measurement error below the height of 100 m. This finding is consistent with the conclusion drawn by Zhang et al. (2018), i.e., the difference between GPS sonde data and DWL measurements obtained near the surface (i.e., < 100 m) is attributable mainly to the radiosonde drift effect. At heights of > 100 m, the balloon will generally drift at a rate equal to the ambient wind speed and therefore the difference between GPS sonde and DWL measurements becomes much smaller. From this perspective, wind measurements obtained by the GPS sonde within 100 m of the ground surface are generally considered unreliable and inaccurate. It can be seen from Figs. 5(f) and 5(g) that the speed of the balloon increased suddenly at 02:02 CST (height: 100 m) and at 05:34 CST (height: 180 m) on August 10. At these instants, the balloon continued to drift horizontally but remained at the same height for a certain period (approximately 10–15 s). This was presumably caused by very strong horizontal winds such as local turbulence or a low-level jet. A similar change can be observed in the DWL 1-s instantaneous speed, whereas the phenomenon is not obvious in the t_{GPS}, 1-min, 2-min, and 10-min average speeds, indicating that averaged results cannot reflect adequately the presence of a low-level jet or turbulence. Furthermore, wind speed measured by the GPS sonde is generally higher than that measured by the DWL because of the inertial acceleration of the balloon. This implies that the DWL 1-s instantaneous result can better reflect atmospheric changes under conditions associated with a low-level jet or turbulence. In addition, the balloons typically spent 38–76 s and traveled horizontally for 0.9–1.6 km when ascending from the ground surface to the maximum observational height of the DWL (i.e., 270 m). Overall, the t_{GPS} average speed of the DWL is in the closest agreement with the GPS sonde measurements, although the vertical variations of the 1-min, 2-min, and 10-min average speeds follow similar trends.

To demonstrate that GPS sonde wind measurements are unreliable and inaccurate at heights < 100 m, quantitative comparison of GPS sonde and DWL wind measurements was undertaken. First, the DWL measurements were arranged into two data sets: one based on heights in the range of 40–270 m and the other based on heights in the range of 100–270 m. For each data set, 1-s instantaneous, t_{GPS}, 1-min, 2-min, and 10-min average speeds were compared with the GPS sonde data acquired at the same heights. The CORR and standard deviation of the wind speed obtained from the two types of instruments were calculated, as illustrated in Fig. 6 using a Taylor diagram. For both sets of DWL data, it can be seen that the t_{GPS} average speed is in best agreement with the corresponding GPS sonde data. At heights in the range of 40–270 m, the level of agreement between the t_{GPS} average speed from the DWL and the GPS sonde data are highest and the associated error is smallest (CORR: 0.88, RMS: 2.69 $\mathrm{m \cdot s^{-1}}$). At heights in the range of 100–270 m, the trend is similar to that found at 40–270 m. However, the CORR between the t_{GPS} average speed and the GPS sonde data are decreased to 0.82 and the RMS is decreased to 2.19 $\mathrm{m \cdot s^{-1}}$ (a reduction of 18.6%). The RMS is still larger than that found in similar comparisons of wind measurements conducted by Pu et al. (2010) regarding Typhoon Nuri (2008) and by Zhang et al. (2018) regarding Tropical Storm Erika (2015), in which RMSs were 1.087 and 1.58

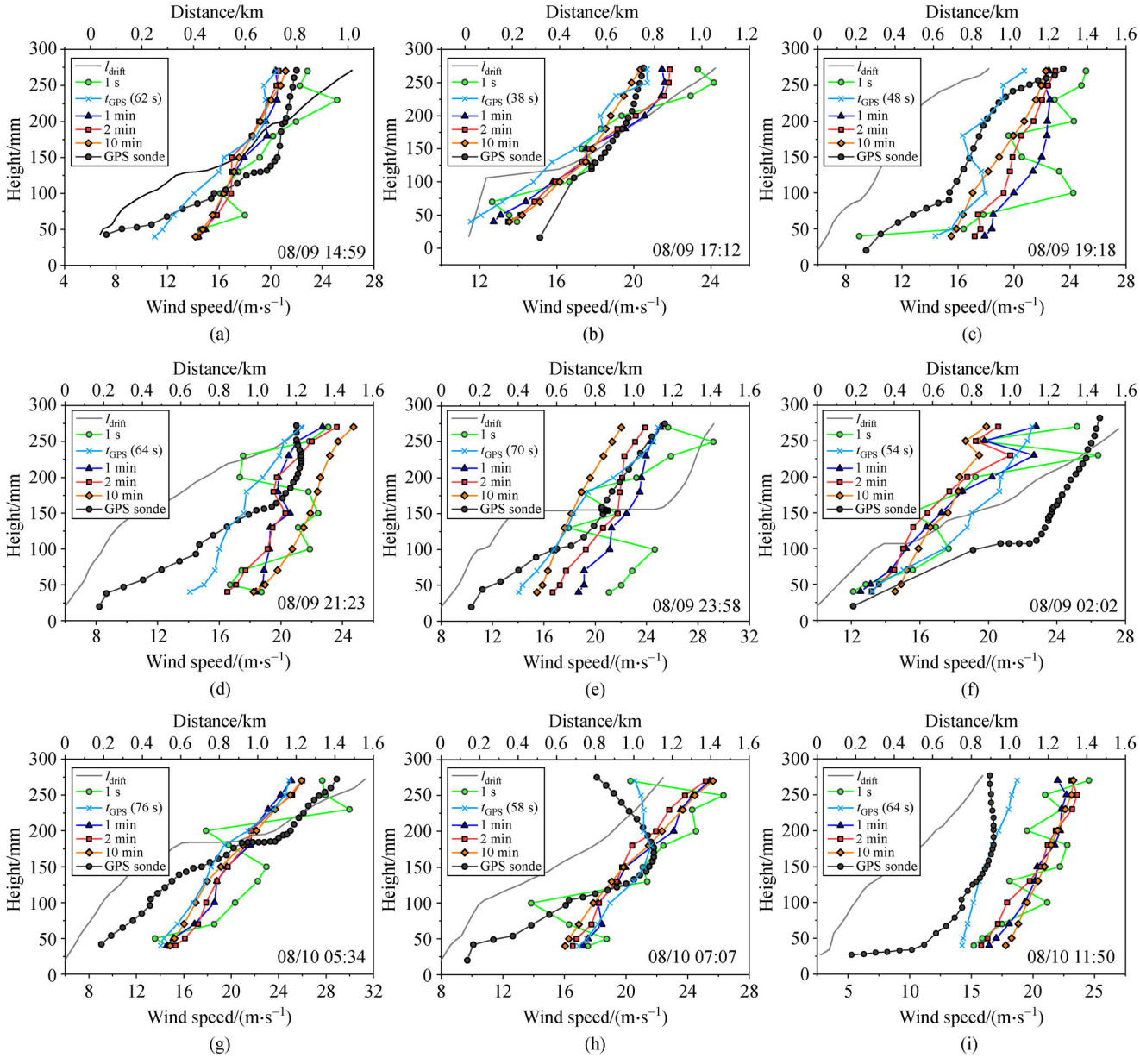

Fig. 5 Comparison of wind speed profiles based on DWL measurements and GPS sonde data at (a) 14:59, (b) 17:12, (c) 19:18, (d) 21:23, and (e) 23:58 CST on August 9, and at (f) 02:22, (g) 05:34, (h) 07:07, and (i) 11:50 CST on August 10. l_{drift} indicates the horizontal drift distance of the sounding balloon during ascent from the ground surface to the height of 270 m. 1 s, t_{GPS}, 1 min, 2 min, and 10 min indicate 1-s instantaneous, t_{GPS}, 1-min, 2-min, and 10-min average wind speeds derived from the DWL measurements and GPS sonde indicates wind speed measured by the GPS sonde.

m·s^{-1}, respectively. The reason is the measurement range in their studies was larger, i.e., from 1200 to 1800 m, and much better agreement can be reached when comparison is made using data acquired at heights > 300 m (further details can be found in Fig. 2 of Pu et al. (2010) and in Fig. 6 of Zhang et al. (2018)). When data from below 100 m are not considered, the RMS is reduced by approximately 20% but the CORR is also reduced by 0.06. This indicates that wind measurements obtained by DWL and GPS sonde are better correlated below 100 m.

To assess how precipitation might affect the performance of DWL wind measurements, the effects of typhoon-induced precipitation on the *CNR*, rate of missing data, and speed measurement error of the DWL were investigated. First, the changing trend of the *CNR* as a function of PI is plotted in Fig. 7, with respect to three different measurement ranges: height ⩽ 100 m, 100 m < height ⩽ 200 m, and 200 m < height ⩽ 270 m. The *CNR* was calculated based on 1-min average results. Here, PI was classified into seven categories, 0–0.01 mm·h^{-1}

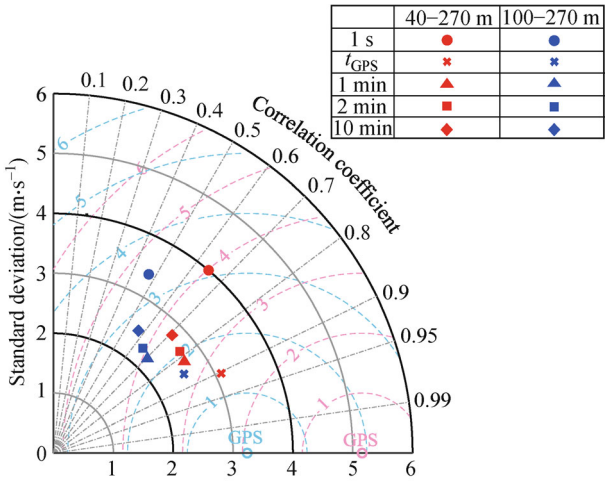

Fig. 6 Taylor diagram of correlation coefficients and standard deviations between DWL and GPS sonde wind speed measurements for two data sets (i.e., 40–270 m and 100–270 m). Note: 1 s, t_{GPS}, 1 min, 2 min, and 10 min denote 1-s instantaneous, t_{GPS}, 1-min, 2-min, and 10-min average DWL wind speeds, respectively.

(clear), 0.01–3 mm·h^{-1} (light rain), 3–6 mm·h^{-1} (moderate rain), 6–12 mm·h^{-1} (heavy rain), 12–30 mm·h^{-1} (rainstorm), 30–90 mm·h^{-1} (heavy rainstorm), and > 90 mm·h^{-1} (severe rainstorm), according to the Group Standard "The grade of rainfall in short-time weather service" (T/CMSA 0013-2019) issued by China Meteorological Services Association. As shown in Fig. 7, the *CNR* generally decreases with the increase of measurement height and increasing PI. During the observation period, the precipitation was predominantly light rain, followed by moderate rain; rainfall with PI equivalent to a severe rainstorm occurred least. Generally, the influence of PI on the *CNR* was different within the various measurement ranges. Specifically, the *CNR* was affected less by low-level precipitation (height ⩽ 100 m), i.e., the *CNR* was generally unchanged, with the majority exceeding –10 dB. In comparison, precipitation affected the *CNR* more at higher levels (height > 200 m) where the *CNR* was decreased remarkably under conditions of heavy or severe rainstorms.

Figure 8 presents the relationship between the rate of missing DWL data and the *CNR* with respect to three measurement ranges: height ⩽ 100 m, 100 m < height ⩽ 200 m, and 200 m < height ⩽ 270 m. Both the rate of missing data and the *CNR* were determined based on 1-min average results. The rate of missing data reduces with the increase of the *CNR*, and the rate at lower levels is less than that at higher levels. It can be seen from Fig. 8(b) that when the *CNR* is higher than –10 dB, the rate of missing data generally remains constant at different heights, i.e., < 5%. When the *CNR* is lower than –15 dB, the rate of missing data at each level increases markedly. Specifically, at heights of ⩽ 100 m, the rate is generally within 30%; however, the rate increases up to 100% at heights > 100 m.

Precipitation affects aerosol concentration in the lower atmosphere. Devara et al. (2003) investigated the relationship between precipitation and aerosol concentration based on observations obtained over a 12-year period. They concluded that aerosol concentration in the lower atmosphere decreases by approximately 40% when precipitation occurs. Given that DWL measurements depend on the presence of small particles as backscattering targets, data availability could be altered by variation of the aerosol concentration in the lower atmosphere (Kumer et al., 2014). The rate of missing DWL data as a function of precipitation over various measurement ranges (height ⩽ 100 m, 100 m < height ⩽ 200 m, and 200 m < height ⩽ 270 m) is shown in Fig. 9. It can be seen that

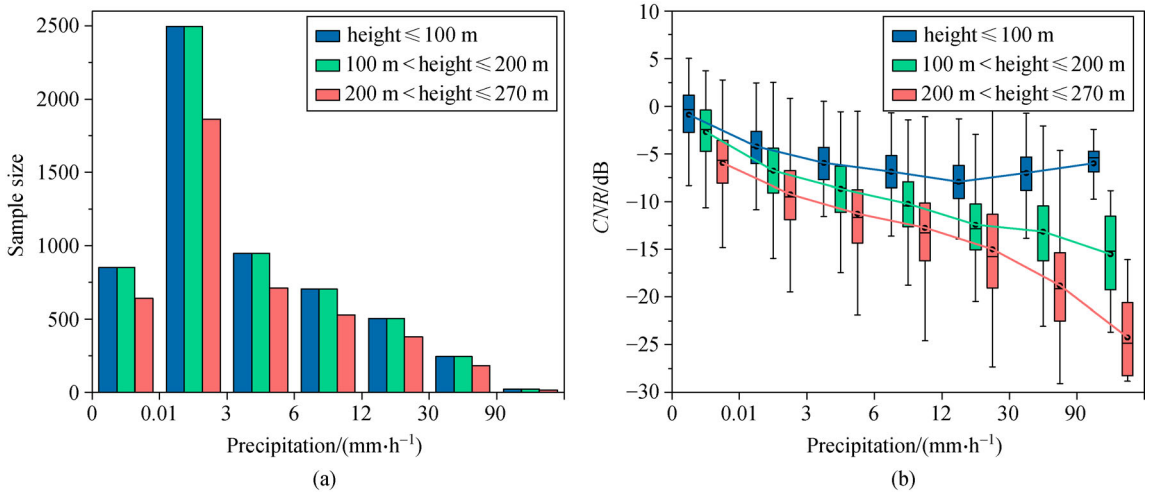

Fig. 7 The *CNR* of the DWL as a function of precipitation: (a) samples, and (b) box plot. Here, PI was classified into seven categories: 0–0.01 mm·h^{-1} (clear), 0.01–3 mm·h^{-1} (light rain), 3–6 mm·h^{-1} (moderate rain), 6–12 mm·h^{-1} (heavy rain), 12–30 mm·h^{-1} (rainstorm), 30–90 mm·h^{-1} (heavy rainstorm), and > 90 mm·h^{-1} (severe rainstorm).

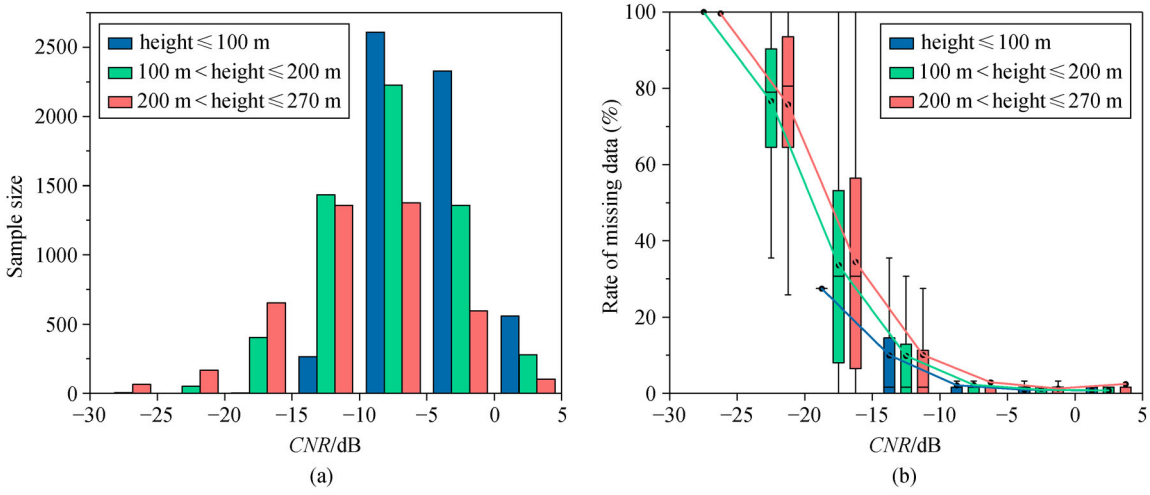

Fig. 8 Rate of missing DWL data as a function of the CNR: (a) samples, and (b) box plot.

the rate of missing data increases with the increase of PI and that the rate at lower levels is less than that higher levels. It can also be determined from Fig. 9(b) that the validity of DWL data at heights of < 100 m is unaffected by precipitation because the associated rate of missing data are constant (i.e., $< 5\%$). However, as the measurement height increases, the rate of missing data becomes increasingly affected by precipitation. Under clear and light rain conditions, the rate of missing data at all heights is $< 5\%$. Under PI conditions of heavy rain and above, the rate of missing data increases rapidly at heights of > 100 m. If the rate of missing data of 50% is used as the critical threshold with which to define the usefulness and validity of DWL data, then DWL data can be considered valid below 300, 200, and 100 m under PI conditions of heavy rain and below, rainstorm to heavy rainstorm, and severe rainstorm, respectively.

To investigate the influence of precipitation on DWL wind speed measurement bias, 1-s instantaneous, t_{GPS}, 1-min, 2-min, and 10-min average values of wind speed bias are plotted against precipitation in Fig. 10. Based on Fig. 10(a), during the period when the GPS sondes collected data in the height range of 0–300 m, precipitation was largely dominated by light–heavy rain, and PI conditions of rainstorm and heavy rainstorm seldom occurred. It can be determined from Fig. 10(b) that no obvious relationship exists between DWL wind speed bias and precipitation, and the t_{GPS} average wind speed bias is in the range from – 5 to 5 $m \cdot s^{-1}$. Based on Figs. 7–10, it can be concluded that precipitation mainly affects the rate of missing DWL data by affecting the *CNR*, but that it has little effect on wind speed bias.

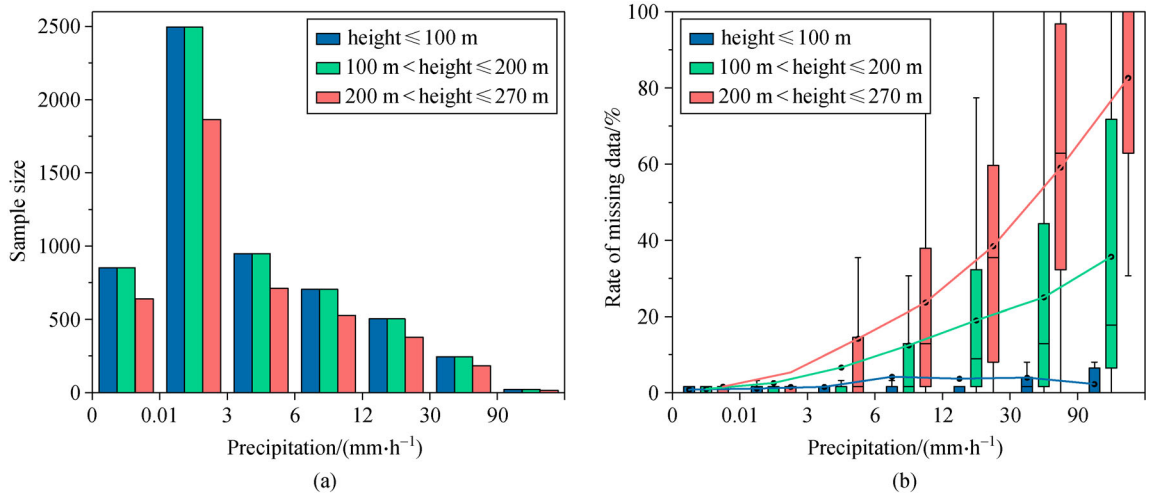

Fig. 9 Rate of missing DWL data as a function of precipitation: (a) samples, and (b) box plot. PI is classified into seven categories: 0–0.01 $mm \cdot h^{-1}$ (clear), 0.01–3 $mm \cdot h^{-1}$ (light rain), 3–6 $mm \cdot h^{-1}$ (moderate rain), 6–12 $mm \cdot h^{-1}$ (heavy rain), 12–30 $mm \cdot h^{-1}$ (rainstorm), 30–90 $mm \cdot h^{-1}$ (heavy rainstorm), and > 90 $mm \cdot h^{-1}$ (severe rainstorm).

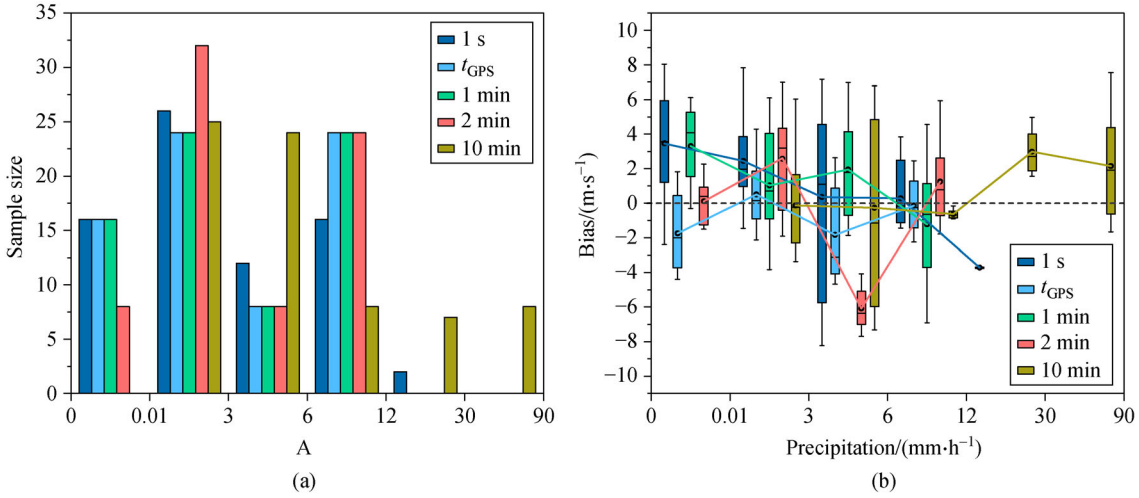

Fig. 10 Horizontal wind speed bias of the DWL as a function of precipitation: (a) samples, and (b) box plot. PI is classified into seven categories: 0–0.01 mm · h^{-1} (clear), 0.01–3 mm · h^{-1} (light rain), 3–6 mm · h^{-1} (moderate rain), 6–12 mm · h^{-1} (heavy rain), 12–30 mm · h^{-1} (rainstorm), 30–90 mm · h^{-1} (heavy rainstorm), and > 90 mm · h^{-1} (severe rainstorm).

4.2 Assessment of wind direction

To validate the reliability of DWL wind direction measurements at heights of > 100 m, the data were classified into two sets: one based on heights in the range of 40–270 m and the other based on heights in the range of 100–270 m. For both sets of data, instantaneous (1-s) and average (t_{GPS}, 1-min, 2-min, and 10-min) wind directions were compared with corresponding GPS sonde data at the same height, and the CORR and standard deviation between these two data sets are illustrated in Fig. 11. The results of both data sets are similar, indicating that the removal of GPS sonde data below 100 m exerts a subtle influence on the measurement error of wind direction. This is mainly because the direction of movement of the balloon is consistent with the direction of the prevailing wind at the initial stage of the ascent (i.e., < 100 m), despite the fact that the speed of movement of the balloon is lower than the horizontal wind speed. For both sets of DWL data, the best level of agreement with the GPS sonde measurements is achieved by the t_{GPS} average wind direction (CORR: 0.94, RMS: 12.4° within 100–270 m). Furthermore, the instantaneous and average wind directions from the DWL are largely the same, and all match well with GPS sonde data. For both data sets, it can also be seen that the CORR is > 0.9 and the RMS error is < 15°, with respect to both the instantaneous and average wind directions. In comparison with the study of Bucci et al. (2018), which compared wind observations acquired in tropical cyclones during 2016 using an airborne DWL and GPS dropsondes, the CORR associated with the data of the current study is similar but the RMS error is much smaller. In summary, irrespective of whether the GPS sonde data acquired at heights of < 100 m are considered, the effect on the wind direction error is insignificant, and the instantaneous and average wind directions obtained from the DWL are generally in reasonable agreement with the GPS sonde data.

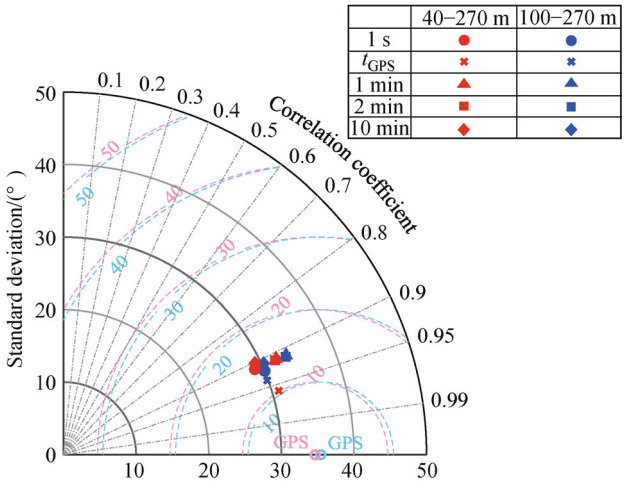

Fig. 11 Taylor diagram of correlation coefficients and standard deviations between DWL and GPS sonde wind direction measurements for two data sets (i.e., 40–270 and 100–270 m). Note: 1 s, t_{GPS}, 1 min, 2 min, and 10 min denote 1-s instantaneous, t_{GPS}, 1-min, 2-min, and 10-min average DWL wind direction, respectively.

To investigate the influence of precipitation on DWL wind direction measurements, the development of 1-s instantaneous, t_{GPS}, 1-min, 2-min, and 10-min average wind direction bias against precipitation is presented in Fig. 12. No obvious trend of change is observed regarding the variation of wind direction bias with precipitation. It can be seen that the t_{GPS} average wind direction bias is generally distributed between –20° and 30°.

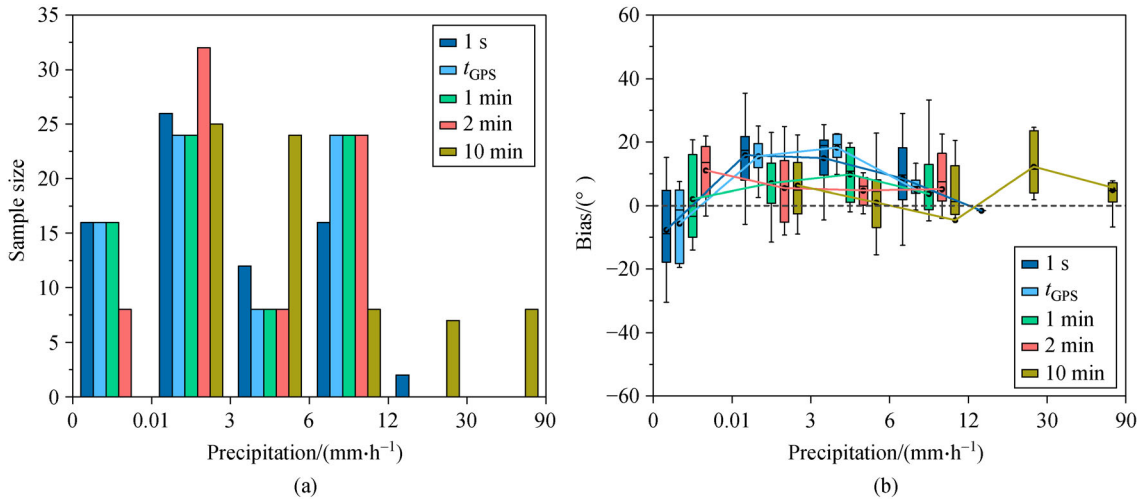

Fig. 12 Horizontal wind direction bias of the DWL as a function of precipitation: (a) samples, and (b) box plot. PI is classified into seven categories: 0–0.01 mm·h^{-1} (clear), 0.01–3 mm·h^{-1} (light rain), 3–6 mm·h^{-1} (moderate rain), 6–12 mm·h^{-1} (heavy rain), 12–30 mm·h^{-1} (rainstorm), 30–90 mm·h^{-1} (heavy rainstorm), and > 90 mm·h^{-1} (severe rainstorm).

4.3 Comparison of DWL, WPR, and GPS sonde data quality

To compare the quality of data collection by the DWL and WPR under the combined effects of typhoon winds and precipitation, both the WPR 10-min average wind speed and the DWL t_{GPS} average wind speed above 100 m from the surface were matched with the GPS sonde instantaneous wind speed at the same height, as presented in Fig. 13. Generally, the WPR measurement is in good agreement with the GPS sonde data within 1.6 km, except at several instants, i.e., 23:58 CST (Fig. 13(e)) on August 9, and 02:22 CST (Fig. 13(f)) and 07:07 CST (Fig. 13(h)) on August 10. These three time instants were all characterized by moderate rain (3–6 mm·h^{-1}) and high winds, implying that WPR data under PI conditions of moderate rain and above is unreliable in high winds. However, the data quality is better under PI conditions of light rain (< 3 mm·h^{-1}), which is consistent with the conclusions reported by Ralph et al. (1995) and by Lambert and Taylor (1998). Based on Section 4.1, it can be concluded that precipitation has insignificant effect on DWL wind speed bias. At heights in the range of 100–300 m, WPR- and DWL-measured wind speeds exhibit similar variation with height. However, in comparison with the WPR data, the DWL-derived measurements present a better match with the GPS sonde data at 23:58 CST on August 9 (Fig. 13(e)), indicating that the DWL wind speed bias is affected relatively less by precipitation.

To reflect quantitatively the level of agreement between both the DWL and the WPR measurements with the GPS sonde data, the CORR and RMS of the DWL and the WPR measurements in relation to the GPS sonde data at heights in the range of 100–300 m are plotted in Fig. 14. Generally, CORR and RMS of the DWL measurements are larger and smaller, respectively, in comparison with the WPR measurements. Specifically, the CORR of the DWL t_{GPS} average wind speed is 0.82, whereas the CORR of the WPR 10-min average wind speed is only 0.64. The RMS of the DWL t_{GPS} average wind speed is 2.19 m·s^{-1}, whereas the RMS of the WPR 10-min average wind speed is 4.32 m·s^{-1}, i.e., nearly twice that of the DWL. Under the combined conditions of typhoon winds and precipitation, the accuracy of the DWL measurements is better than that of the WPR measurements at heights in the range of 100–300 m. Wolfe et al. (2005) compared the performance of a DWL with that of a WPR under normal wind conditions and reached similar conclusions, i.e., the DWL data produced a wind field that was more accurate in the range of 500 m.

5 Conclusions and discussion

This study conducted verification of the applicability and accuracy of DWL-measured winds. The data were collected during Super Typhoon Lekima (2019) as part of a field experiment conducted in Zhoushan, Zhejiang Province (China) by Shanghai Typhoon Institute of China Meteorological Administration. The DWL observations were compared with those derived from GPS sondes launched from the same location. Specifically, DWL-measured 1-s instantaneous, t_{GPS}, 1-min, 2-min, and 10-min average wind speeds and directions were compared with instantaneous winds obtained from the GPS sondes at heights of up to 300 m. Furthermore, we also investigated the impact of precipitation on the *CNR* and rate of missing DWL data.

Comparison of the wind profiles derived from the DWL and GPS sondes revealed a substantial difference in the

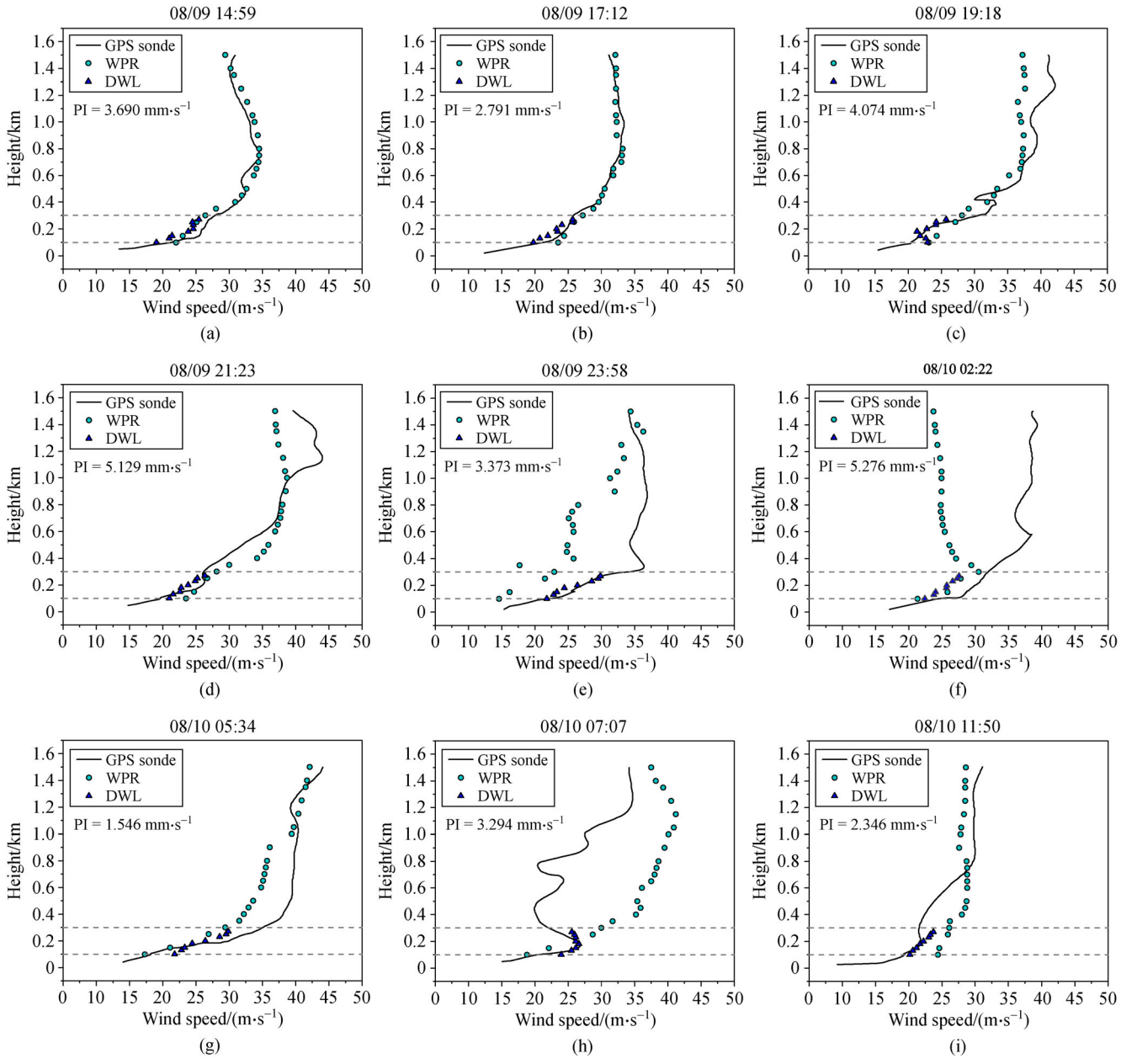

Fig. 13 Comparison of WPR 10-min average wind speed and GPS sonde data at (a) 14:59, (b) 17:12, (c) 19:18, (d) 21:23, and (e) 23:58 CST on August 9, and at (f) 02:22, (g) 05:34, (h) 07:07, and (i) 11:50 CST on August 10.

measurements at heights of < 100 m, which was attributable primarily to the drift effect of the sounding balloon. It is therefore believed that wind speed measured by a GPS sonde at heights of < 100 m is unreliable. Above 100 m, the best level of agreement with the GPS sonde wind speed measurements was achieved by the DWL-measured t_{GPS} average wind speed (CORR: 0.82, RMS: 2.19 m·s^{-1}), whereas the 1-s instantaneous wind speed produced the worst level of agreement. From this perspective, the t_{GPS} average wind speed, which is the wind speed time-averaged during the GPS sonde ascent from the ground surface to the height of 270 m, is recommended for use as the benchmark for verification of the WindCube V2 DWL. As for wind direction, the best level of agreement was found for the t_{GPS} average wind direction (CORR: 0.94, RMS: 12.4° within 100–270 m), and our analysis revealed reasonable agreement between the DWL measurements (including instantaneous and averaged wind directions) and the GPS sonde data (CORR: > 0.9, RMS: < 15°). Furthermore, it was established that precipitation has little influence on the DWL-measured wind direction, and the bias of the t_{GPS} average wind direction is generally distributed between –20° and 30°.

During typhoon conditions, PI affects the rate of missing

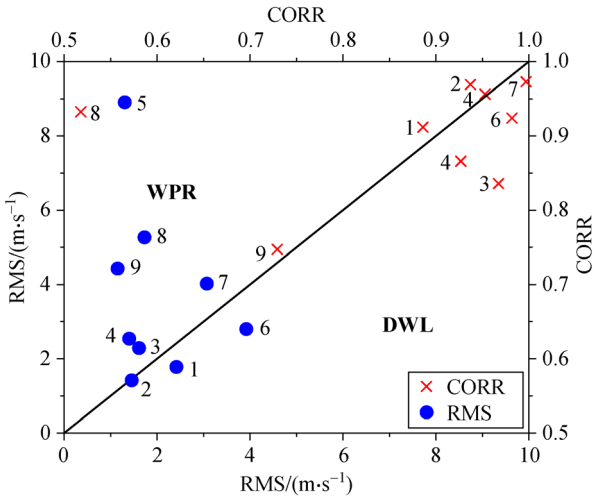

Fig. 14 The CORR and RMS of DWL and WPR measurements in relation to GPS sonde data at heights in the range of 100–300 m. CORR denotes the correlation coefficient, and RMS denotes the root mean square. The numbers 1–10 correspond to specific time instants at 14:59, 17:12, 19:18, 21:23, and 23:58 CST on August 9 and at 02:22, 05:34, 07:07, and 11:50 CST on August 10.

DWL data mainly through changing the value of the *CNR*. However, PI has little effect on the wind speed bias of the DWL measurements. Specifically, the *CNR* decreases with the increase of both measurement height and PI. At heights of < 100 m, the *CNR* is affected little by precipitation and it remains nearly constant. However, precipitation exerts a major influence on the *CNR* at heights of > 200 m, where the *CNR* is reduced drastically in association with heavy or severe rainstorms. Moreover, the rate of missing data increases with the increase of both measurement height and PI. The validity of DWL data within 100 m is generally unaffected by precipitation and the associated rate of missing data are largely constant (i.e., $< 5\%$). If the rate of missing data of 50% is considered the critical threshold for defining the validity of DWL data, then DWL data can be considered valid below 300, 200 and 100 m under PI conditions of heavy rain and below (< 12 mm·h^{-1}), rainstorm to heavy rainstorm (12–90 mm·h^{-1}), and severe rainstorm (> 90 mm·h^{-1}), respectively.

Comparison of the wind profiles based on the DWL, WPR, and GPS sonde measurements revealed that the RMS of the DWL measurements is nearly half that of the WPR measurements within the height range of 100–300 m, indicating that the DWL wind data are more accurate than the WPR wind data.

Future work will concentrate on cooperative field experiments of typhoon boundary layer in which several DWLs and GPS sondes will be deployed at different locations (Alford et al., 2020; Zhang et al., 2020). The simultaneous measurements of the typhoon boundary layer acquired by the multiple DWLs and GPS sondes will support further investigation of the wind structure of the typhoon boundary layer for both scientific and engineering applications.

Acknowledgements This work was supported by the National Key R&D Program of China (No. 2018YFB1501104), Key Program for International S&T Cooperation Projects of China (No. 2017YFE0107700), National Natural Science Foundation of China (Grant No. 41805088), and Natural Science Foundation of Shanghai (No. 18ZR1449100). We are grateful to Rong Zhu, Peter Dodge and an anonymous reviewer for their constructive comments on the original version of the submitted manuscript. We also thank James Buxton MSc from Liwen Bianji, Edanz Group China, for editing the English text of this manuscript.

References

Agrawal G P (2010). Fiber-Optic Communication Systems, 4th ed. New York: John Wiley & Sons, Inc

Alford A A, Zhang J A, Biggerstaff M I, Dodge P, Marks F D, Bodine D J (2020). Transition of the hurricane boundary layer during the landfall of Hurricane Irene (2011). J Atmos Sci: JAS-D-19-0290.1

Barat J, Cot C (1995). Accuracy analysis of Rubsonde-GPS wind sounding system. J Appl Meteorol, 34(5): 1123–1132

Bu Z, Zhang Y, Chen S, Pan G, Lu L, He C (2014). Noise modeling by the trend of each range gate for coherent Doppler LIDAR. Opt Eng, 53 (6): 063109.063101–063109.063106

Bucci L R, O'Handley C, Emmitt G D, Zhang J A, Ryan K, Atlas R (2018). Validation of an airborne doppler wind lidar in tropical cyclones. Sensors (Basel), 18(12): 4288

Courtney M, Wagner R, Lindelöw P (2008). Testing and comparison of lidars for profile and turbulence measurements in wind energy. In: IOP Conference Series Earth and Environmental Science, 1(1): 012021

Davis J, Collier C, Davies F, Burton R, Pearson G, Di Girolamo P (2013). Vertical velocity observed by Doppler lidar during cops–a case study with a convective rain event. Meteorol Z (Berl), 22(4): 463–470

Devara P, Raj P, Pandithurai G, Dani K, Maheskumar R (2003). Relationship between lidar-based observations of aerosol content and monsoon precipitation over a tropical station, Pune, India. Meteorol Appl, 10(3): 253–262

Drew D R, Barlow J F, Lane S E (2013). Observations of wind speed profiles over Greater London, UK, using a Doppler lidar. J Wind Eng Ind Aerodyn, 121(121): 98–105

Emmitt G D (2010). Airborne Doppler wind lidar investigations of western pacific typhoon genesis and evolution. IEEE International Geoscience & Remote Sensing Symposium, 2010

Frehlich R G, Kavaya M J (1991). Coherent laser radar performance for general atmospheric refractive turbulence. Appl Opt, 30(36): 5325–5352

Gasch P, Wieser A, Lundquist J K, Kalthoff N (2020). An LES-based airborne Doppler lidar simulator and its application to wind profiling in inhomogeneous flow conditions. Atmos Meas Tech, 13(3): 1609–1631

GB/T 19201–2006 (2006). Grade of Tropical Cyclones. General Administration of Quality Supervision Inspection and Quaratine of the People's Republic China. Beijing: Standards Press of China

Hannon S M (2000). Autonomous infrared Doppler radar: airport surveillance applications. Phys Chem Earth Pt B, 25(10–12): 1005–1011

Köpp F, Schwiesow R L, Werner C (1984). Remote measurements of boundary-layer wind profiles using a CW Doppler Lidar. J Appl Meteorol, 23(1): 148–154

Kumer V, Reuder J, Furevik B R (2014). A comparison of LiDAR and radiosonde wind measurements. Energy Procedia, 53: 214–220

Lambert W C, Taylor G E (1998). Data quality assessment methods for the eastern range 915 MHz wind profiler network. NASA Contractor Report NASA/CR-1998-207906

Lhermitte R, Atlas D (1961). Precipitaion motion by pulse Doppler radar. In: 9th Weather Radar Conference. Boston: American Meteological Society, 218–223

Li J L, Yu X (2017). LiDAR technology for wind energy potential assessment: demonstration and validation at a site around Lake Erie. Energy Convers Manage, 144: 252–261

Li J L, Wang X F, Yu X (2018). Use of spatio-temporal calibrated wind shear model to improve accuracy of wind resource assessment. Appl Energy, 213: 469–485

Matvienko G, Grishin A, Zilberman A (1995). Correlation lidar measurements of meteorological characteristics in conditions of atmospheric condensation. In: European Symposium on Optics for Environmental & Public Safety. International Society for Optics and Photonics

Peña A, Hasager C B, Gryning S E, Courtney M, Antoniou I, Mikkelsen T (2009). Offshore wind profiling using light detection and ranging measurements. Wind Energy (Chichester Engl), 12(2): 105–124

Powell M D, Vickery P J, Reinhold T A (2003). Reduced drag coefficient for high wind speeds in tropical cyclones. Nature, 422(6929): 279–283

Pu Z X, Zhang L, Emmitt G D (2010). Impact of airborne Doppler wind lidar profiles on numerical simulations of a tropical cyclone. Geophys Res Lett, 37(5): L05801

Rabadan G J, Schmitt N P, Pistner T, Rehm W (2010). Airborne lidar for automatic feedforward control of turbulent in-flight phenomena. J Aircr, 47(2): 392–403

Ralph F M, Neiman P J, van de Kamp D W, Law D C (1995). Using spectral moment data from NOAA's 404-MHz radar wind profilers to observe precipitation. Bull Am Meteorol Soc, 76(10): 1717–1739

Roadcap J R, Mcnicholl P J, Jr E H T, Laird M H (2001). Comparison of CO_2 Doppler lidar and GPS rawinsonde wind velocity measurements. Proceedings of Spie the International Society for Optical Engineering, 4376: 141–152

Smith D A, Harris M, Coffey A S, Mikkelsen T, Jorgensen H E, Mann J, Danielian G (2006). Wind lidar evaluation at the Danish wind test site in Hovsore. Wind Energy (Chichester Engl), 9(1–2): 87–93

Träumner K, Wieser A, Grenzhäuser J, Kottmeierr C (2009). Advantages of a coordinated scanning Doppler lidar and cloud radar system for wind measurements. In: 4th symposium on lidar atmospheric applications, Arizona, USA

Werner C (1985). Fast sector scan and pattern recognition for a cw laser Doppler anemometer. Appl Opt, 24(21): 3557–3564

Wolfe D E, Fairall C W, Intrieri J M, Ratterree M, Tucker S (2005). Shipboard multisensor wind profiles from NEAQS 2004: radar wind profiler, high resolution Doppler lidar, GPS rawinsonde. In: 13th Symposium on Meteorological Observations and Instrumentation, Joint Poster Session JP2.27

Ying M, Zhang W, Yu H, Lu X Q, Feng J X, Fan Y X, Zhu Y T, Chen D Q (2014). An overview of the China Meteorological Administration Tropical Cyclone Database. J Atmos Ocean Technol, 31(2): 287–301

Yu H, Chen L S (2019). Impact assessment of landfalling tropical cyclones: introduction to the special issue. Front Earth Sci, 13(4): 669–671

Zhang J A, Atlas R, Emmitt G D, Bucci L, Ryan K (2018). Airborne Doppler wind lidar observations of the tropical cyclone boundary layer. Remote Sens, 10(6): 825

Zhang J A, Dunion J P, Nolan D S (2020). *In situ* observations of the diurnal variation in the boundary layer of mature hurricanes. Geophys Res Lett, 47 (3)

Zheng C, Gao Z, Rui Z, Chen X (2015). Application of T639 forecasting wind field around Taiwan Island. Journal of PLA University of Science & Technology, 16(1): 80–88